

Part 2—Quantum Chemistry Studies of Peroxynitrous Acid
(HOONO)

The work presented in Part 2 of this thesis (Chapter 3) has been published as part of our theoretical paper on torsion-torsion coupling and vibrational spectroscopy of HOONO. Reproduced in part with permission from McCoy et al.⁴³ Copyright 2010 American Chemical Society.

Chapter 3—A 3-Dimensional Potential Energy Surface and Dipole Moment Surface for Modeling the Torsion-Torsion Coupling in cis-cis HOONO

Abstract

The reaction of the hydroxyl radical (OH) with the nitrogen dioxide radical (NO_2) can form one of two products: peroxyxynitrous acid (HOONO), or nitric acid (HONO_2). Because HOONO is a temporary reservoir for OH and NO_2 , while HONO_2 is a permanent reservoir, the branching ratio of these two reaction channels is atmospherically significant. Previous experiments have measured the OH-stretch cavity ringdown spectra of HOONO and HONO_2 formed from $\text{OH} + \text{NO}_2$ to assess the branching ratio. However, the torsional modes of HOONO are coupled to the OH-stretch, leading to a series of sequence bands that complicate the OH-stretch spectrum. These sequence bands must be accounted for in order to obtain a quantitatively correct branching ratio. This chapter describes a 3-dimensional potential energy surface and dipole moment surface for HOONO to study the torsion/torsion coupling to the OH stretch. Geometries and energies were computed at the CCSD(T)/cc-pVTZ level of theory and basis, as a function of the HOON and OONO dihedral angles and the OH bond length. Dipole moments were then calculated at the CCSD/aug-cc-pVDZ level of theory and basis. The resulting surfaces were used to compute the wavefunctions, energies, and two simulated spectra of HOONO: the OH stretch spectrum, and the HOON and OONO torsional spectrum. These data were used in conjunction with the previous cavity ringdown spectra to obtain the true branching ratio for the two channels of $\text{OH} + \text{NO}_2$, and to make assignments in the matrix spectrum of HOONO.

Introduction

The reaction of the hydroxyl radical (OH) with nitrogen dioxide (NO₂) is a very important reaction in the troposphere. As stated in Chapter 1, HO_x and NO_x radicals catalyze tropospheric ozone formation, causing air pollution and health hazards. Both OH and NO₂ are formed from industrial and automotive emissions: OH from the oxidation of methane, and NO₂ directly from combustion engine and industrial plant emissions.¹⁻³ Because of the large impact on air quality, it is important to understand how OH and NO₂ will react with each other in the atmosphere.

Until thirty years ago, it was assumed that OH + NO₂ formed only nitric acid (HONO₂).^{56, 57} However, Robertshaw et al. noticed that their data did not fit to a single termolecular falloff curve. They suggested the possibility of two reaction pathways, one of which was a “weakly bound state.”¹³ Spectroscopic studies by Lee (matrix IR) identified this product as peroxyntrous acid (HOONO).⁵⁸⁻⁶¹ Thus, there are two reaction pathways for OH + NO₂:



The geometry and energetics of HOONO has been determined by many theoretical and experimental studies.^{12, 16, 42, 43, 62-72} The ground state of HOONO is bound by 19.6 kcal mol⁻¹ below the dissociation limit to OH + NO₂. In contrast, HONO₂ is 47.2 kcal mol⁻¹ below the dissociation limit (Figure 3.1).¹²

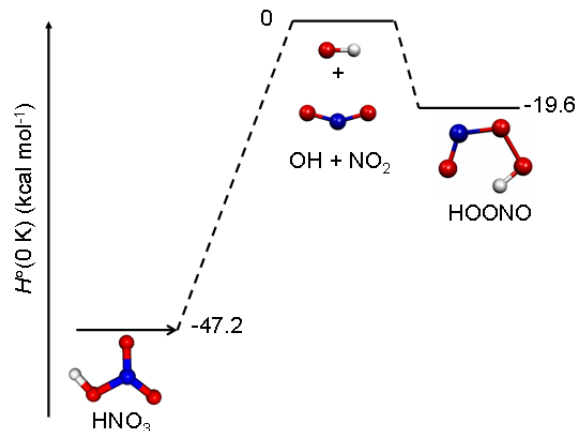


Figure 3.1. Potential energy surface for OH + NO₂. From Mollner et al.¹² Reprinted with permission from AAAS.

HOONO exists as three conformers: cis-cis, cis-perp, and trans-perp (Figure 3.2). The labels cis, perp, and trans refer to HOON and OONO dihedral angles of 0°, 90°, and 180° respectively. Of the three conformers, cis-cis HOONO is the most stable, 3 kcal mol⁻¹ lower than the trans-perp conformer.⁷⁰ The energy stabilization of the cis-cis conformer arises from the internal hydrogen bond formed between the terminal H and O atoms. While the cis-cis and trans-perp conformers have been located numerous times in theoretical studies, the existence of the cis-perp conformer is still debated. Depending on the level of theory, the cis-perp isomer is either a local minimum that supports at least one bound state,⁴² or is simply a shelf along the potential energy surface that does not support any bound states, but will have increased wavefunction amplitude.⁶⁸

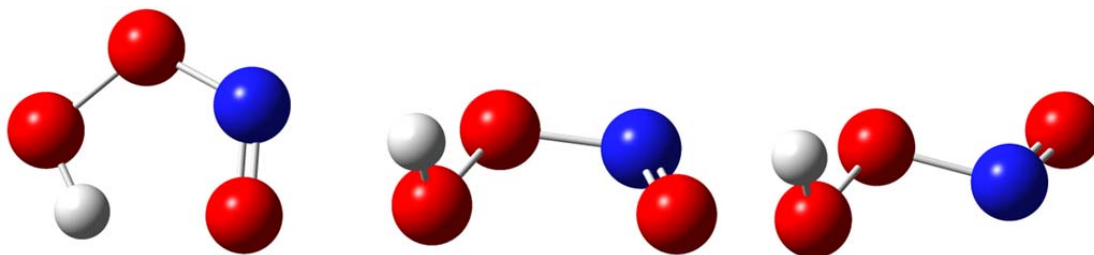


Figure 3.2. The three conformers of HOONO: cis-cis (left), cis-perp (center), and trans-perp (right).

Because HOONO is so weakly bound, the question arises as to whether HOONO formation is atmospherically relevant. Initial spectroscopic studies used Fourier transform infrared (FTIR) spectroscopy, and could not detect HOONO, leading to the conclusion that HOONO was not atmospherically important.⁷³ In the last decade, more sensitive gas phase experiments have been performed, utilizing cavity ringdown spectroscopy (CRDS) to directly detect the OH stretch fundamental^{12, 15} and overtone spectra,^{14, 42, 74} and action spectroscopy to detect the OH stretch overtone spectra.^{67, 68, 70, 75, 76} These experiments have detected gas phase HOONO in both the cis-cis and trans-perp conformers. Additionally, Li et al. were able to observe the cis-perp conformer using a pulsed supersonic expansion. The abundance of positive gas phase detections leads to the conclusion that HOONO is likely formed in the atmosphere.

The fate of HOONO in the atmosphere is very different than HONO₂. Because HOONO is weakly bound, it will rapidly dissociate back to OH + NO₂. This means that HOONO acts as a temporary sink for HO_x and NO_x. In contrast, HONO₂ is very strongly bound, and acts as a permanent sink for HO_x and NO_x. Knowing the amount of HOONO formed will give us a better understanding of the HO_x and NO_x budgets, and will allow us to refine our atmospheric models. We therefore are interested in determining the branching ratio (α) of the two channels of Reactions 3.1 and 3.2, defined as

$$\alpha(T, p) = \frac{k_{HOONO}(T, p)}{k_{HONO_2}(T, p)}. \quad (3.3)$$

The most recent experiment to evaluate Equation 3.3 was performed by Mollner et al.¹² This experiment used laser induced fluorescence (LIF) measurement of OH disappearance to obtain the overall rate constant for OH + NO₂, and CRDS measurements

of cis-cis HOONO and HONO₂ to obtain $\alpha(298K,p)$. The CRDS measurements made use of the OH stretch spectra of both species (cis-cis HOONO at 3306 cm⁻¹, and HONO₂ at 3551 cm⁻¹). It should be noted that typical OH stretch frequencies are found in the range 3500–3700 cm⁻¹. The large red shift in OH stretch frequency for cis-cis HOONO arises from the internal hydrogen bond.^{15, 42} The branching ratio was then calculated by using the integrated CRDS peak intensities:

$$\alpha(298K,p) = \frac{\int \text{Abs}_{\text{HOONO}}}{\int \text{Abs}_{\text{HONO}_2}} \times \frac{\sigma_{\text{HONO}_2}}{\sigma_{\text{HOONO}}}, \quad (3.4)$$

where $\frac{\sigma_{\text{HONO}_2}}{\sigma_{\text{HOONO}}}$ is taken from high level calculations (CCSD(T)/ANO).¹⁶

The one remaining problem with the kinetic analysis presented so far is that the OH stretch normal mode in cis-cis HOONO is coupled to the HOON and OONO torsional modes. This coupling arises from the internal hydrogen bond: the same hydrogen bond that is responsible for HOONO's large red shift in the OH stretch frequency. As the HOON or OONO dihedral angles increase (due to excitation of the two torsional normal modes), the internal hydrogen bond breaks, and the OH stretch frequency will increase. The end result is the formation of sequence bands in the spectrum. A sequence band of a transition is defined as the same change in energy quanta as the fundamental transition, but with the initial molecule not in the ground state. For example, the fundamental transition of the OH stretch is defined as

$$(n_{\text{OH}} = 0, n_{\text{HOON}} = 0, n_{\text{OONO}} = 0, \dots) \rightarrow (n_{\text{OH}} = 1, n_{\text{HOON}} = 0, n_{\text{OONO}} = 0, \dots). \quad (3.5)$$

In Equation 3.5, $\Delta n_{\text{OH}} = 1$, while all of the other normal modes remain in their ground state. One of the possible sequence bands involves a HOONO molecule that starts off

with one quantum of energy in the HOON torsion. The sequence band is therefore defined as

$$(n_{OH} = 0, n_{HOON} = 1, n_{OONO} = 0, \dots) \rightarrow (n_{OH} = 1, n_{HOON} = 1, n_{OONO} = 0, \dots). \quad (3.6)$$

In Equation 3.6, Δn_{OH} is still 1, but the HOON torsion has one quantum of energy in both the initial and final states. Similar sequence bands can be defined for any of the other normal modes, or combinations of the normal modes.

The torsional modes of HOONO have somewhat low frequencies, on the order of 300 cm^{-1} and 500 cm^{-1} for the HOON and OONO modes respectively. At room temperature, significant amounts of HOONO will be torsionally excited, and the OH stretch frequency of these excited molecules will increase. If the OH stretch frequency increases too much, OH stretch intensity will be shifted outside of the main HOONO spectroscopic band, and the simple integration in Equation 3.4 will not account for this intensity. **If the effects of sequence band formation are not explicitly accounted for, the branching ratio calculated from the CRDS experiment will be too low.**

Normal mode coupling also significantly affects the matrix spectrum of Zhang et al.¹⁶ Zhang's experiment measures the HOONO spectrum in the region $400\text{-}1000 \text{ cm}^{-1}$. This spectroscopic region contains the torsional fundamentals, overtones, and combination bands. Because the torsional modes are coupled, assignment of the peaks is not straightforward. Explicitly modeling the coupling between the two normal modes will allow for a more confident assignment of the matrix spectrum.

There have been two previous studies on normal mode coupling in cis-cis HOONO. McCoy et al. examined how the HOON torsional mode coupled to the OH stretch.⁴² Using a CCSD(T)/cc-pVTZ potential energy surface and a HF/aug-cc-pVTZ

dipole moment surface, McCoy determined that 15% of the OH stretch intensity is shifted into sequence bands. Matthews et al. examined how both the HOON torsional mode and HOO bend mode coupled to the OH stretch.⁶⁷ Matthews concluded that the HOO angle had minimal effect on top of the HOON torsional motion. Both studies examined the minimum energy path (MEP), allowing all other degrees of freedom to relax. Until our current work,⁴³ no studies have examined how the OONO torsional mode couples to the OH stretch. Since this mode will also break the internal hydrogen bond, we expect that it is necessary to explicitly account for this mode in order to accurately account for sequence band formation.

This thesis chapter presents a 3-dimensional potential energy surface and dipole moment surface for HOONO, as a function the OH bond length, the HOON dihedral angle, and the OONO dihedral angle. The shape of the potential energy surface and minimum energy path is analyzed to determine the extent of the coupling. Our potential energy surface will allow us to assess whether cis-perp conformer of HOONO exists as a shelf or as a local minimum. The energy levels and wavefunctions (calculated by Professor Anne McCoy) are then used to predict the sequence band positions and intensities in the OH stretch spectrum, and to predict the torsional fundamental and overtone spectrum.⁴³ The sequence bands are used to derive a correction factor for Mollner's calculated branching ratio.¹² The simulated torsional spectrum allows us to propose assignments for Zhang's matrix spectrum.¹⁶

Methods

Our main goals for this study are to obtain the OH stretch spectrum and the torsional spectrum for cis-cis HOONO. In order to obtain these, we need to map out approximately 6000 cm^{-1} of the potential energy surface. This will be enough to simulate the OH stretch spectrum as well as the torsional spectrum. Mapping the surface out this far will also allow us to assess whether the cis-perp conformer of HOONO exists as a local minimum or as a shelf.

All quantum chemistry computations (geometry optimizations, dipole moments) were carried out in Gaussian 98W,⁷⁷ Gaussian 03,⁷⁸ and Gaussian 03W.⁷⁹ We used four single processor, single core, Windows XP PCs (Caltech) and one multiprocessor Unix Beowulf cluster (Ohio State) to perform the calculations. Generation of wavefunctions, energy levels, and transition intensities was performed by Professor Anne McCoy (Ohio State), and will only be briefly discussed in this chapter to put the spectroscopy results into context.

Generation of Potential Energy Surface and Dipole Moment Surface

Our three dimensional potential energy surface was a function of the HOON dihedral angle (τ_{HOON}), the OONO dihedral angle (τ_{OONO}), and the OH bond length (r_{OH}). Our approach adiabatically separated the OH stretch motion from the torsional motion. We allowed τ_{HOON} to vary from 0° to 180° , and τ_{OONO} from 0° to 50° . We then optimized the geometries at each pair of dihedral angles, allowing the remaining degrees of freedom to relax. Geometries were optimized at the CCSD(T)/cc-pVTZ level of theory and basis.⁸⁰⁻⁸³ This level of theory has been used in previous studies of HOONO,⁴² and has

been shown to give results in good quantitative agreement with experiment. We did not directly optimize geometries at this level of theory. To use CPU time more efficiently, the optimizations were carried out in a series of steps. Optimizations were carried out in the order MP2/cc-pVDZ,^{84, 85} CCD/cc-pVDZ, CCSD(T)/cc-pVDZ, and finally CCSD(T)/cc-pVTZ. We then calculated the single point energies at values of r_{OH} of $r_e - 0.15 \text{ \AA}$ to $r_e + 0.25 \text{ \AA}$ in increments of 0.05 \AA , where r_e is the equilibrium OH bond length at each pair of τ_{HOON} and τ_{OONO} , keeping all other degrees of freedom fixed.

We did not optimize every combination of dihedral angles in the range ($0^\circ < \tau_{\text{HOON}} < 180^\circ$, $0^\circ < \tau_{\text{OONO}} < 50^\circ$). Instead, we used an irregular grid of points. More geometries were calculated near the cis-cis HOONO potential minimum, and fewer geometries were calculated at points further away. The rationale for this choice of grid and the convergence of our surface will be explained in the *Results* section.

It was initially unclear what level of theory and basis set were appropriate for calculating the dipole moment surface. Previous calculations were found to have used Hartree-Fock theory, which is woefully inadequate for describing the dipole moment of HOONO.⁴² We performed diagnostic tests on the dipole moment of cis-cis geometry of HOONO, varying r_{OH} from $r_e - 0.30 \text{ \AA}$ to $r_e + 0.30 \text{ \AA}$ in steps of 0.05 \AA , using six levels of theory and basis set combinations: QCISD/cc-pVDZ,⁸⁶ QCISD/aug-cc-pVDZ, QCISD/cc-pVTZ, CCSD/cc-pVDZ, CCSD/aug-cc-pVDZ, and CCSD/cc-pVTZ. As a result of these diagnostic tests (see the *Results* section for details), we calculated the entire dipole moment surface at the CCSD/aug-cc-pVDZ level of theory and basis. The dipole moments were converted into the principal axis coordinates to permit comparison to the previous dipole calculations of McCoy et al.⁴²

Simulation of Spectra

Fitting of the potential energy surfaces, generation of wavefunctions and energy levels, and simulation of the OH stretch and torsional spectra was the work of Professor Anne McCoy (Ohio State). The procedure and results are only briefly summarized here to put the branching ratio correction and torsional spectral assignments into context. A full description of the methods used can be found in the literature.⁴³

The energies obtained from the geometry optimizations were fit to the function

$$V(r_{OH}, \tau_{HOON}, \tau_{OONO}) = \sum_{n=0,2-4} \sum_{m=0}^{23} c_{n,m} y^n f_m(\tau_{HOON}, \tau_{OONO}), \quad (3.7)$$

where

$$y = 1 - \exp[-\alpha \Delta r_{OH}], \quad (3.8)$$

α is a constant, and the f_m are a series of trigonometric functions (sines and cosines) of τ_{HOON} and τ_{OONO} .

The dipoles were converted to an Eckart frame, then fit to the following two equations (for the a/b component and the c component respectively)

$$\mu_{a/b}(r_{OH}, \tau_{HOON}, \tau_{OONO}) = \sum_{n=0}^3 \sum_{m=0}^{23} d_{n,m}^{(a)/(b)} \Delta r_{OH}^n f_m(\tau_{HOON}, \tau_{OONO}), \quad (3.9)$$

$$\mu_c(r_{OH}, \tau_{HOON}, \tau_{OONO}) = \sum_{n=0}^3 \sum_{m=1}^{23} d_{n,m}^c \Delta r_{OH}^n g_m(\tau_{HOON}, \tau_{OONO}), \quad (3.10)$$

where the f_m are the same functions used in Equation 3.7, and the g_m are slightly different trigonometric functions based on the A'' symmetry of the c component of the dipole. These functional forms are then used to solve the Schrödinger equation in two steps: first the one-dimensional equation for the OH stretch, then the two-dimensional equation for the two dihedral angles.

The resulting wavefunctions can be combined with the dipole moment surface to generate the transition moments necessary for simulating the OH stretch spectrum:

$$\vec{\mu}_{\nu_{OH\leftarrow 0}}(\tau_{HOON}, \tau_{OONO}) = \langle \psi_0 | \vec{\mu} | \psi_{OH} \rangle \quad (3.11)$$

Similar equations are used to determine the transition moments for the torsional spectrum.

Results

Although the potential energy surface that we generated is in three dimensions, it is easiest to first consider two dimensions in order to observe the torsion-torsion coupling between the HOON and OONO torsional normal modes. The coupling of the torsional modes to the OH stretch is most easily shown by examination of the sequence bands present in the OH stretch spectrum. Therefore, we present the results in four parts. First, we present the potential energy surface as a function of the two dihedral angles, and comment on the coupling of the two torsional normal modes. Second, we show how the OH stretch potential energy surface varies as a function of τ_{HOON} and τ_{OONO} , indicating that the OH stretch is coupled to both torsional motions. Third, we show the logic behind the choice of the level of theory used for computing the dipole moment surface. Fourth, we present the wavefunctions, energy levels, and OH stretch and torsional spectra (all calculated by Professor McCoy), showing the effects of the coupling between the torsional modes and the OH stretch.

Torsional Potential Energy Surface

The plot of the potential energy surface of HOONO as a function of the HOON and OONO dihedral angles is illustrated in Figure 3.3. This surface makes use of the adiabatic approximation for r_{OH} , assuming that the OH bond length adjusts to its equilibrium value at each point along the surface. The cis-cis conformer of HOONO is located at the center of the plot. The black dots represent the points where geometries were optimized and energies were calculated. The points along the line $\tau_{\text{OONO}} = 0^\circ$ were taken from previously reported calculations.⁴² The grey stars represent the final points calculated, which will become important during the discussion about the choice of points along our irregular grid.

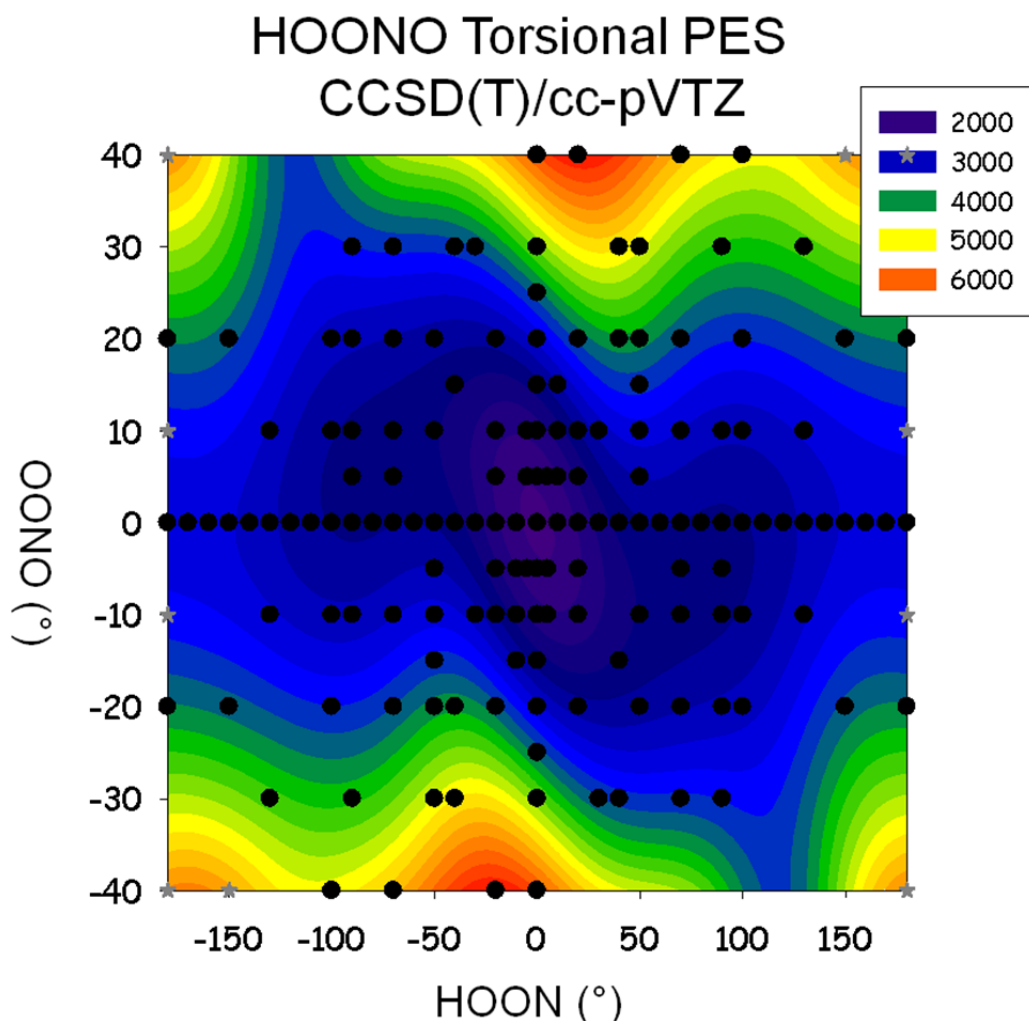


Figure 3.3. Potential energy surface of HOONO as a function of the two torsional angles τ_{HOON} and τ_{ONOO} . All other degrees of freedom were allowed to relax, including the OH bond length (r_{OH}). Energies were computed at selected points on the plot (black and silver dots) the CCSD(T)/cc-pVTZ level of theory and basis. Energies reported in cm^{-1} . Adapted with permission from McCoy et al.⁴³ Copyright 2010 American Chemical Society.

Before describing the shape and features of the potential energy surface, it is worthwhile to discuss the rationale behind the irregular grid of points used, and why this grid gives an accurate result for the PES. The goal of using the irregular grid was to save computational time. A single CCSD(T) geometry optimization took approximately one week of CPU time, whether on one node of Ohio State's Beowulf cluster or on one of our Windows XP computers. Thus, careful selection of points to optimize was critical for

completing this computational study in a reasonable amount of time. More geometries were chosen close to the bottom of the potential energy well (i.e., closer to cis-cis HOONO) to accurately map out the parts of the surface most likely to affect the torsional coupling and the sequence band formation in the OH stretch spectrum. We also chose more points near the cis-perp shelf/potential minimum, in order to accurately assess the contribution of cis-perp HOONO to the spectroscopy of HOONO. Fewer points were chosen outside of the cis-cis and cis-perp regions because the two torsional modes uncouple from each other, making the potential energy surface easier to fit. We did not optimize geometries where the energy would be above 6000 cm^{-1} relative to cis-cis HOONO, as these points would have minimal effect on the simulated spectra.

To evaluate whether the potential energy surface was converging, we performed fits to incomplete surfaces, with each surface containing two to six new points. We then computed the RMS error for the fit, and were satisfied with the number of points on the surface when the RMS error stopped changing. This criterion was satisfied when the final points of the potential energy surface were computed (grey stars on Figure 3.3). Considering all three dimensions (r_{OH} , τ_{HOON} , τ_{OONO}), the RMS error for the potential was 28 cm^{-1} . Along the torsional PES shown in Figure 3.3, the RMS error is an order of magnitude lower, 2.6 cm^{-1} .⁴³ The accurate mapping of the potential well combined with the convergence of the fit to the surface allows us to proceed with our analysis.

There are several features of the torsional potential energy surface that should be noted. The first feature is the shape of the potential energy well near the cis-cis HOONO minimum. The well is off-axis from the HOON and OONO dihedral angles, indicating that the two torsional normal modes involve motions that simultaneously affect both

angles. As the HOONO molecule moves out of the cis-cis well, the two torsions uncouple from each other, and motions along the HOON and OONO dihedral angles are independent from each other. This is most easily seen for $\tau_{\text{HOON}} > 100^\circ$.

Second, we note the large barrier to torsional motion along the OONO axis compared to the HOON axis. The energy difference between cis-cis HOONO and the trans-cis transition state ($\tau_{\text{HOON}} = 180^\circ$, $\tau_{\text{OONO}} = 0^\circ$) is only 1212 cm^{-1} . In contrast, consider a much smaller change in the OONO dihedral angle. The energy difference between cis-cis HOONO and ($\tau_{\text{HOON}} = 0^\circ$, $\tau_{\text{OONO}} = 40^\circ$) is 4202 cm^{-1} . Our potential energy surface indicates that the barrier to the trans-perp region of HOONO is greater than 6000 cm^{-1} , in agreement with previous theoretical and experimental studies.^{42, 67, 68, 70, 75, 76, 87, 88}

Third, our potential energy surface sheds light on the nature of the cis-perp conformer of HOONO. Previous theoretical attempts at locating a stable cis-perp minimum have been unsuccessful.^{16, 65, 67, 68, 74} McCoy et al. are able to find a local minimum for cis-perp HOONO when τ_{OONO} is restricted to 0° .⁴² However, because of this restriction, they note that they “do not ascribe too much significance to the predicted depth (or lack) of the well”. Our potential energy surface is a superset of McCoy’s surface, allowing us to determine the nature of the cis-perp minimum that they calculated. The cis-perp minimum observed in McCoy’s study does not lie along the minimum energy path (MEP) out of the cis-cis HOONO potential energy well. Rather, for a dihedral angle of $\tau_{\text{HOON}} = 90^\circ$, the minimum energy occurs near $\tau_{\text{OONO}} = -5^\circ$ (not 0°). Furthermore, our surface indicates that along our MEP, there is no local minimum at

$\tau_{\text{HOON}} = 90^\circ$; rather, the potential energy surface forms a shelf. Based on our potential energy surface, the cis-perp conformer of HOONO cannot be isolated.

Despite the lack of a local minimum at $\tau_{\text{HOON}} = 90^\circ$, we do not conclude that cis-perp HOONO is spectroscopically unimportant. Our surface is in agreement with previous theoretical studies: the potential energy surface has a shelf near $\tau_{\text{HOON}} = 90^\circ$. As will be shown in the *Wavefunctions* section, the potential energy shelf will give rise to a buildup of wavefunction intensity in the torsionally excited states of HOONO. We would therefore expect cis-perp character to be present in the experimental spectra, in agreement with the action spectroscopy experiments.⁷⁶

Comparison of CCSD(T) and B3LYP Torsional Potential Energy Surface

Figure 3.4 shows the 2D torsional potential energy surface of HOONO calculated at B3LYP/6-31+G(d,p) (left) and CCSD(T)/cc-pVTZ (right). B3LYP energies were calculated with regular spacing, $\Delta\tau_{\text{HOON}} = 10^\circ$, $\Delta\tau_{\text{OONO}} = 10^\circ$. The contour scales for both plots are equal (4000 cm^{-1} range), so the colors correspond to the same energies relative to cis-cis HOONO.

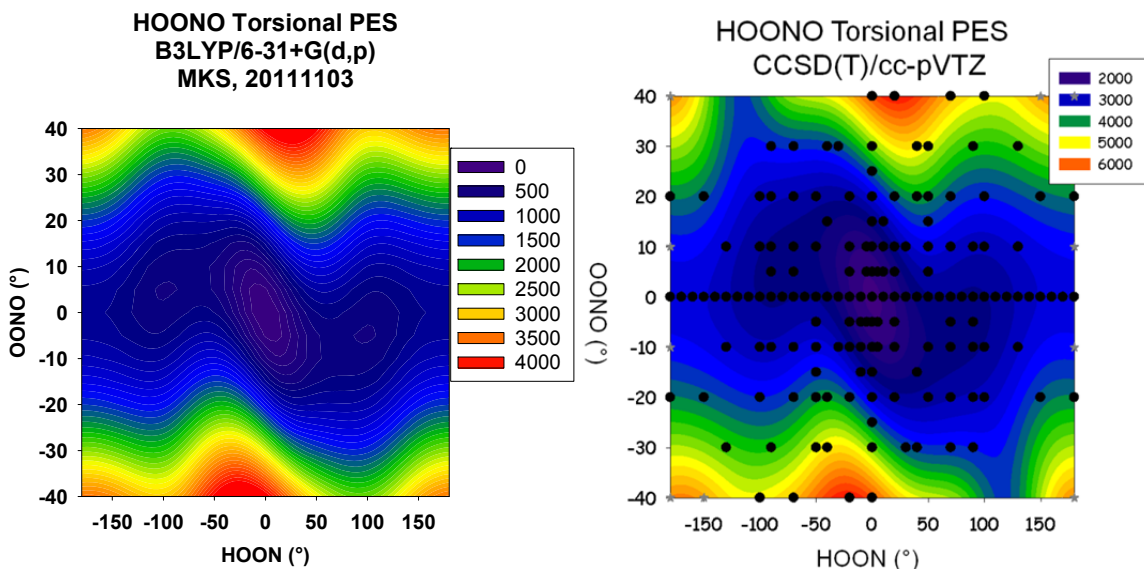


Figure 3.4. Potential energy surface of HOONO as a function of the two torsional angles τ_{HOON} and τ_{OONO} . Left: B3LYP/6-31+G(d,p). Right: CCSD(T)/cc-pVTZ.⁴² All other degrees of freedom were allowed to relax, including the OH bond length (r_{OH}). Energies on the B3LYP surface were calculated at regular intervals ($\Delta\tau_{\text{HOON}} = 10^\circ$, $\Delta\tau_{\text{OONO}} = 10^\circ$). Energies on the CCSD(T) surface were computed at selected points on the plot (black and silver dots). All energies reported in cm^{-1} . Right panel adapted with permission from McCoy et al.⁴³ Copyright 2010 American Chemical Society.

We note two features of interest when comparing the two potential energy surfaces. First, the potential energy well is more off-axis in the lower level B3LYP calculation than in the higher level CCSD(T) calculation, indicating that the two methods disagree with respect to the strength of mode coupling. Second, the barriers to the trans-perp region at $(100^\circ, -40^\circ)$ and $(-100^\circ, 40^\circ)$ are higher in the B3LYP calculation (2000 cm^{-1}) than in the CCSD(T) calculation (1000 cm^{-1}). This is likely an artifact in the CCSD(T) calculation due to the choice of points in the irregular grid.

It is useful to compare the qualitative features of our CCSD(T) potential energy surface to lower levels of theory, as done in Figure 3.4. There has been recent interest in the energetics and spectroscopy of ROONO molecules,⁸⁹⁻⁹⁴ and potential future studies may include hydroxylated ROONO (HOROONO). Similar to HOONO, torsional

coupling may play a significant role in the energetics and spectroscopy of HOROONO, and explicit modeling of the torsional potential energy surfaces will be necessary to obtain accurate energy levels and simulated spectra. Depending on the size of the R group, it may become too computationally expensive to perform CCSD studies, and quantum chemists will be limited to lower levels of theory. The surfaces in Figure 3.4 show that the qualitative features of torsional mode coupling can be reproduced at lower levels of theory. However, the differences in the extent of coupling will produce quantitatively different energy levels and infrared spectra. It may be worthwhile to perform a systematic study to determine the minimum level of theory and basis required to obtain an accurate description of HOONO and HOROONO energetics.

OH Stretch Potential Energy Surface

As stated earlier, we calculated an OH stretch potential for each geometry on the torsional potential energy surface. Rather than present all of the OH stretch potentials in this section, we choose a few potential energy slices that illustrate how the OH stretch motion is coupled to the two torsional motions. The easiest way to do this is to compare the OH stretch potential at the cis-cis minimum to two other points: one with $\tau_{\text{HOON}} > 0^\circ$, and one with $\tau_{\text{OONO}} > 0^\circ$.

Figure 3.5 shows plots of $V(r_{\text{OH}}) - V(r_e)$ vs $r_{\text{OH}} - r_e$ for three pairs of dihedral angles: ($\tau_{\text{HOON}} = 0^\circ$, $\tau_{\text{OONO}} = 0^\circ$) (a), ($\tau_{\text{HOON}} = 90^\circ$, $\tau_{\text{OONO}} = 0^\circ$) (b), and ($\tau_{\text{HOON}} = 0^\circ$, $\tau_{\text{OONO}} = 40^\circ$) (c). Each plot shows the potential over the range $-0.15 \text{ \AA} < r_{\text{OH}} - r_e < 0.25 \text{ \AA}$. Additionally, all three potential energy slices are shown overlaid on each other, with the minimum of each potential energy slice set to 0 cm^{-1} (d).

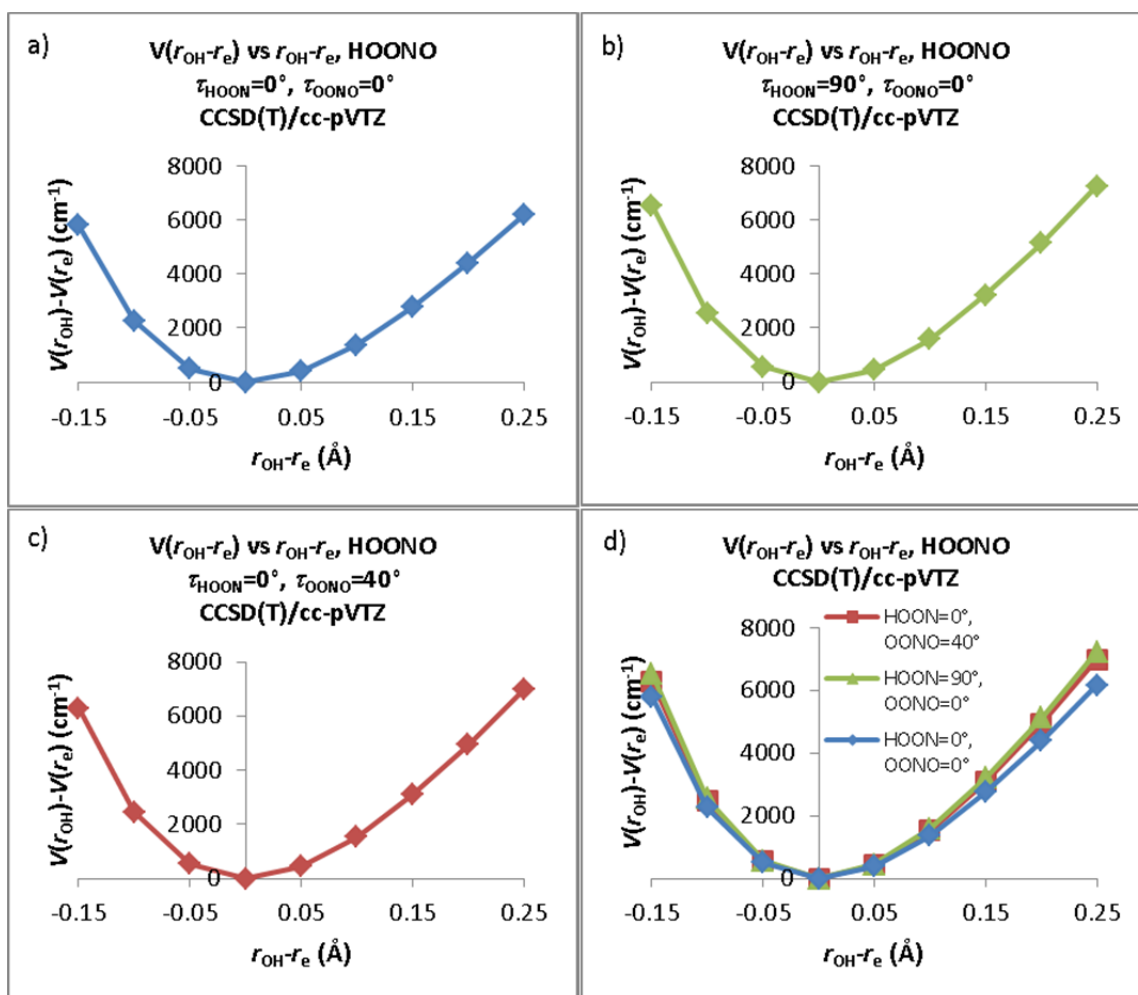


Figure 3.5. Potential energy of HOONO (in cm^{-1}) vs OH bond length change ($r_{\text{OH}} - r_e$) for three sets of dihedral angles: ($\tau_{\text{HOON}} = 0^\circ$, $\tau_{\text{OONO}} = 0^\circ$) (a), ($\tau_{\text{HOON}} = 90^\circ$, $\tau_{\text{OONO}} = 0^\circ$) (b), and ($\tau_{\text{HOON}} = 0^\circ$, $\tau_{\text{OONO}} = 40^\circ$) (c). In part d, all three plots are overlaid, with the minima of each plot set to 0 cm^{-1} . Energies were calculated at the CCSD/cc-pVTZ level of theory and basis.

Figure 3.5d allows us to analyze the curvature of each potential energy surface, and determine how increasing the two dihedral angles will affect the OH stretch. We notice that an increase in either of the dihedral angles causes the potential energy well to become narrower. This is due to the internal hydrogen bond in cis-cis HOONO breaking. The end result would be an increase in OH stretch frequency, in agreement with the

physical picture of HOONO built up over the last decade. While previous work showed that the HOON torsion was coupled to the OH stretch, we show that the OONO torsion also couples to the OH stretch (Figures 3.5c and 3.5d), and should be explicitly accounted for when modeling torsional coupling.

Calculation of the Dipole Moment Surface

In contrast to the potential energy surface described above, the 3-dimensional dipole moment surface reported in this thesis is not a superset of the 2-dimensional surface in McCoy's 2005 paper. The reason for this was that McCoy's dipole moments were actually calculated at a lower level of theory (HF/aug-cc-pVTZ) than reported in their paper (QCISD/aug-cc-pVTZ).⁴² We eventually decided to recalculate the entire dipole moment surface at CCSD/aug-cc-pVDZ.

Before discussing the logic that went into choosing the level of theory for our surface, it is instructive to go through how we determined that the dipoles were being calculated incorrectly. There were two pieces of evidence that showed how the original dipole surface was incorrectly calculated. First, we took two of the original Gaussian 03 input files used for McCoy's 2005 paper and changed only the level of theory for the dipole calculation: HF, QCISD, QCISD(T), CCSD, and CCSD(T). The two files only differed by basis set (cc-pVTZ and aug-cc-pVTZ). Table 3.1 shows the resulting dipole moments from these calculations. **Each calculation for a given basis set yields the same dipole moment, independent of the level of theory.** This result is clearly absurd: the electronic properties of the molecule change as a function of the level of theory, and therefore the electric dipole should also change. The problem is that the previous input

files did not include the `Density=Current` keyword, which indicates that the QCISD or CCSD wavefunctions should be used in calculation of molecular properties.⁷⁷ Without this keyword, the HF wavefunction is instead used. Therefore, the previously reported dipole surface used the Hartree-Fock dipoles. As will be shown later in this section, this level of theory is inadequate for describing the dipole surface.

Table 3.1. Dipole moments for HOONO with $\tau_{\text{HOON}} = 70^\circ$, $\tau_{\text{OONO}} = 20^\circ$, $r_{\text{OH}} = r_e - 0.15 \text{ \AA}$, calculated without the `Density=Current` keyword

Level of Theory	Basis	μ_x (Debye)	μ_y (Debye)	μ_z (Debye)	$ \mu $ (Debye)
HF	cc-pVTZ	0.2609	-0.4355	1.6088	1.6870
QCISD	cc-pVTZ	0.2609	-0.4355	1.6088	1.6870
QCISD(T)	cc-pVTZ	0.2609	-0.4355	1.6088	1.6870
CCSD	cc-pVTZ	0.2609	-0.4355	1.6088	1.6870
CCSD(T)	cc-pVTZ	0.2609	-0.4355	1.6088	1.6870
HF	aug-cc-pVTZ	0.2538	-0.4540	1.5570	1.6416
QCISD	aug-cc-pVTZ	0.2538	-0.4540	1.5570	1.6416
QCISD(T)	aug-cc-pVTZ	0.2538	-0.4540	1.5570	1.6416
CCSD	aug-cc-pVTZ	0.2538	-0.4540	1.5570	1.6416
CCSD(T)	aug-cc-pVTZ	0.2538	-0.4540	1.5570	1.6416

The second piece of evidence that the previous calculations were not run at the reported level of theory comes from unsuccessful attempts to correct the previous calculations. Since the original goal was to run the dipole moment surface at QCISD/aug-cc-pVTZ, we attempted to re-run some of the original dipole files using the `Density=Current` keyword. Each calculation crashed while using this keyword. The reason for this crash was that the QCISD/aug-cc-pVTZ and CCSD/aug-cc-pVTZ calculations require more memory than the 16 GB scratch space limit inherent to the 32-bit version of Gaussian. In contrast, HF/aug-cc-pVTZ does stay within the 16 GB limit, explaining why McCoy's previous calculations did not crash. There are two

solutions to this problem. One would be to run the calculations on a 64-bit version of Gaussian (or another 64-bit computational chemistry package). However, even with access to these programs, QCISD/aug-cc-pVTZ and CCSD/aug-cc-pVTZ are simply too expensive to feasibly use for calculation of our dipole moment surface, given the computing resources available at the time of this study (2006-2008). **This is why we devoted time to the second solution: finding another level of theory and basis at which to compute the dipole moment surface.**

The levels of theory that are within reason for our computing resources are QCISD and CCSD. We do not include perturbative triples (T) for either method because the inclusion of triples makes all of the dipole derivative computations numerical instead of analytic, and therefore too expensive. We have three basis sets that we can examine: cc-pVDZ, aug-cc-pVDZ, and cc-pVTZ. This allows us to determine the effect of adding diffuse and polarization functions, and the effect of triple zeta vs double zeta. We therefore calculate the dipoles using the following six methods (abbreviations listed in parentheses):

- QCISD/cc-pVDZ (Q/D)
- QCISD/aug-cc-pVDZ (Q/aD)
- QCISD/cc-pVTZ (Q/T)
- CCSD/cc-pVDZ (C/D)
- CCSD/aug-cc-pVDZ (C/aD)
- CCSD/cc-pVTZ (C/T)

To ensure that the electronic populations and dipole moments were computed from the correlated wavefunction rather than the SCF wavefunction, the keyword `Density=Current` was used in the route line of the input file. The Cartesian dipoles reported by Gaussian were then transformed into the normal mode coordinates. Dipoles were calculated varying the OH bond length from $r_{\text{OH}} = r_e - 0.3\text{\AA}$ to $r_{\text{OH}} = r_e + 0.3\text{\AA}$, in

steps of 0.05\AA , essentially repeating McCoy's HF/aug-cc-pVTZ (H/aT) calculations.⁴²

By transforming the dipoles into the normal mode coordinates and using these r_{OH} values, we can directly assess whether the dipole moment surface is improved by a higher level of theory. Dipole derivatives at $r_{\text{OH}} = r_e$ were approximated by Equation 3.12:

$$\frac{d\mu_i}{dr_{\text{OH}}} \approx \frac{[\mu_{i,r_e+0.05\text{\AA}} - \mu_{i,r_e-0.05\text{\AA}}]}{0.1\text{\AA}}, \quad (3.12)$$

where $\mu_{i,r}$ is the value of the i component of the dipole at $r_{\text{OH}} = r$.

The values of μ_a are tabulated in Table 3.2, and plotted in Figure 3.6. At $r_{\text{OH}} = r_e$, the HF/aug-cc-pVTZ dipole is 58% larger than the QCISD/aug-cc-pVDZ dipole, and 28% larger than the CCSD/aug-cc-pVTZ dipole. Similarly, the HF/aug-cc-pVTZ dipole derivative is twice as large as the QCISD/aug-cc-pVDZ dipole derivative, and 45% larger than the CCSD/aug-cc-pVDZ dipole derivative. Simultaneously, we notice that within the QCISD and CCSD methods, changing the basis set has a much smaller impact on the calculated dipole moments or the dipole derivative. The level of theory is the largest factor in determining the electric dipole properties. Based on the tabulated dipole values, the aug-cc-pVDZ and cc-pVTZ calculations give similar dipole and dipole derivative data at both levels of theory.

Table 3.2. Calculated values of μ_a (debye) for cis-cis HOONO, $r_{\text{OH}} = r_e - 0.3 \text{ \AA}$ to $r_e + 0.3 \text{ \AA}$

$r_{\text{OH}}-r_e$	$\mu_a(\text{Q/D})$	$\mu_a(\text{Q/aD})$	$\mu_a(\text{Q/T})$	$\mu_a(\text{HF/aT})$	$\mu_a(\text{C/D})$	$\mu_a(\text{C/aD})$	$\mu_a(\text{C/T})$
-0.30	0.482	0.424	0.437	0.598	0.556	0.503	0.509
-0.25	0.481	0.424	0.436	0.613	0.559	0.508	0.512
-0.20	0.485	0.429	0.440	0.635	0.568	0.517	0.520
-0.15	0.494	0.438	0.448	0.663	0.582	0.533	0.534
-0.10	0.507	0.453	0.463	0.697	0.601	0.554	0.553
-0.05	0.525	0.473	0.482	0.738	0.625	0.580	0.579
0.00	0.547	0.498	0.507	0.786	0.655	0.613	0.611
0.05	0.574	0.528	0.536	0.841	0.690	0.651	0.649
0.10	0.605	0.562	0.571	0.904	0.731	0.696	0.693
0.15	0.640	0.601	0.611	0.975	0.777	0.746	0.742
0.20	0.679	0.644	0.654	1.054	0.828	0.802	0.798
0.25	0.720	0.691	0.702	1.141	0.883	0.864	0.859
0.30	0.764	0.741	0.752	1.236	0.943	0.931	0.924
$d\mu_a/dr_{\text{OH}}$ (at $r_{\text{OH}}=r_e$)	0.491	0.545	0.545	1.031	0.648	0.711	0.696

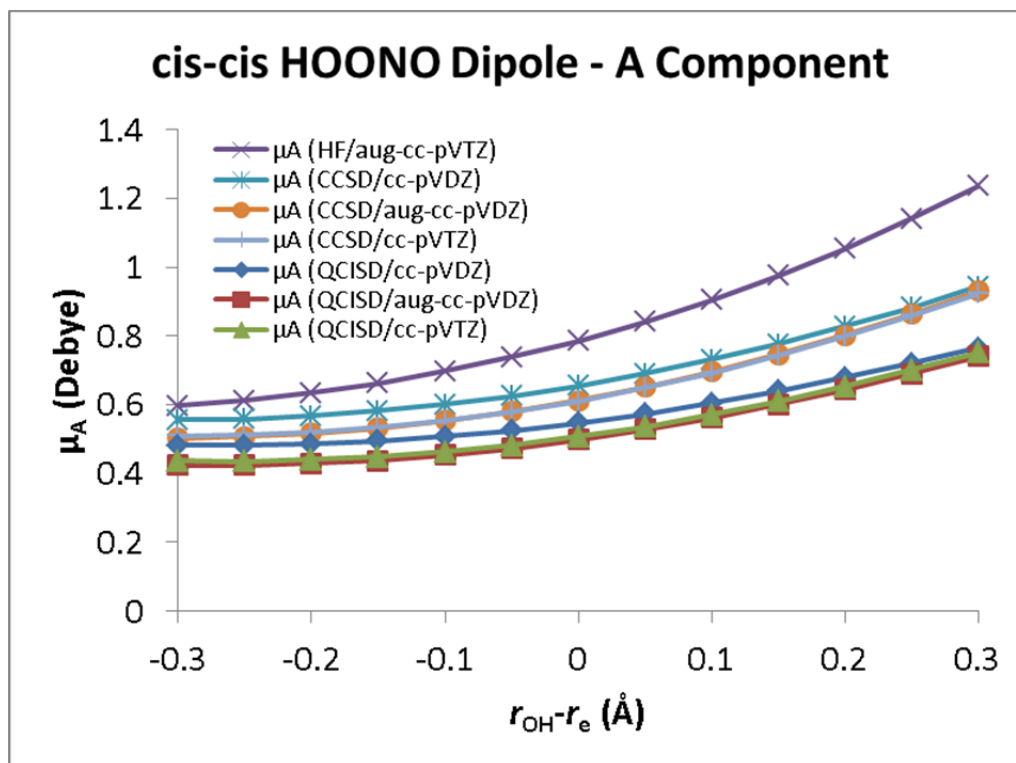


Figure 3.6. μ_a (Debye) for cis-cis HOONO, for $r_{\text{OH}} = r_e - 0.3 \text{ \AA}$ to $r_e + 0.3 \text{ \AA}$, at seven combinations of level of theory and basis. The HF/aug-cc-pVTZ data are taken from McCoy et al.⁴² The dipole value and dipole derivative are most sensitive to the level of theory, with a slight contribution from changing the basis set. In both the CCSD and QCISD cases, the aug-cc-pVDZ and cc-pVTZ bases give similar results.

Having considered the A component of the dipole, we now turn our attention to the B component. The values of μ_a are tabulated in Table 3.3, and plotted in Figure 3.7. We notice that near $r_{\text{OH}} = r_e$, μ_b is relatively constant across methods compared to the A component (10% difference between the largest and smallest values of μ_b). However, we also notice that the HF/aug-cc-pVTZ dipole derivative is roughly 50% larger than the derivative calculated by other methods. The QCISD and CCSD methods give somewhat similar results. In both cases, the aug-cc-pVDZ dipoles are closer to the cc-pVDZ dipoles at small r_{OH} , and closer to the cc-pVTZ dipoles at large r_{OH} . Additionally, the cc-pVDZ and cc-pVTZ dipole derivatives at $r_{\text{OH}} = r_e$ agree with each other, while the aug-cc-pVDZ derivative is 10% smaller.

Table 3.3. Calculated values of μ_b (Debye) for cis-cis HOONO, $r_{\text{OH}} = r_e - 0.3 \text{ \AA}$ to $r_e + 0.3 \text{ \AA}$

$r_{\text{OH}}-r_e$	$\mu_b(\text{Q/D})$	$\mu_b(\text{Q/aD})$	$\mu_b(\text{Q/T})$	$\mu_b(\text{HF/aT})$	$\mu_b(\text{C/D})$	$\mu_b(\text{C/aD})$	$\mu_b(\text{C/T})$
-0.30	-0.604	-0.596	-0.576	-0.508	-0.626	-0.619	-0.596
-0.25	-0.649	-0.634	-0.617	-0.555	-0.671	-0.658	-0.637
-0.20	-0.692	-0.670	-0.656	-0.602	-0.715	-0.694	-0.677
-0.15	-0.733	-0.704	-0.694	-0.649	-0.756	-0.729	-0.714
-0.10	-0.771	-0.736	-0.730	-0.695	-0.794	-0.762	-0.751
-0.05	-0.806	-0.767	-0.764	-0.741	-0.829	-0.792	-0.785
0.00	-0.837	-0.795	-0.796	-0.787	-0.861	-0.821	-0.817
0.05	-0.866	-0.821	-0.826	-0.833	-0.890	-0.848	-0.848
0.10	-0.892	-0.845	-0.855	-0.880	-0.916	-0.872	-0.876
0.15	-0.915	-0.867	-0.881	-0.929	-0.939	-0.895	-0.902
0.20	-0.935	-0.888	-0.905	-0.979	-0.959	-0.916	-0.927
0.25	-0.953	-0.908	-0.929	-1.031	-0.976	-0.936	-0.950
0.30	-0.969	-0.928	-0.951	-1.086	-0.992	-0.956	-0.972
$\frac{d\mu_b}{dr_{\text{OH}}}$ (at $r_{\text{OH}} = r_e$)	-0.606	-0.541	-0.625	-0.924	-0.611	-0.552	-0.630

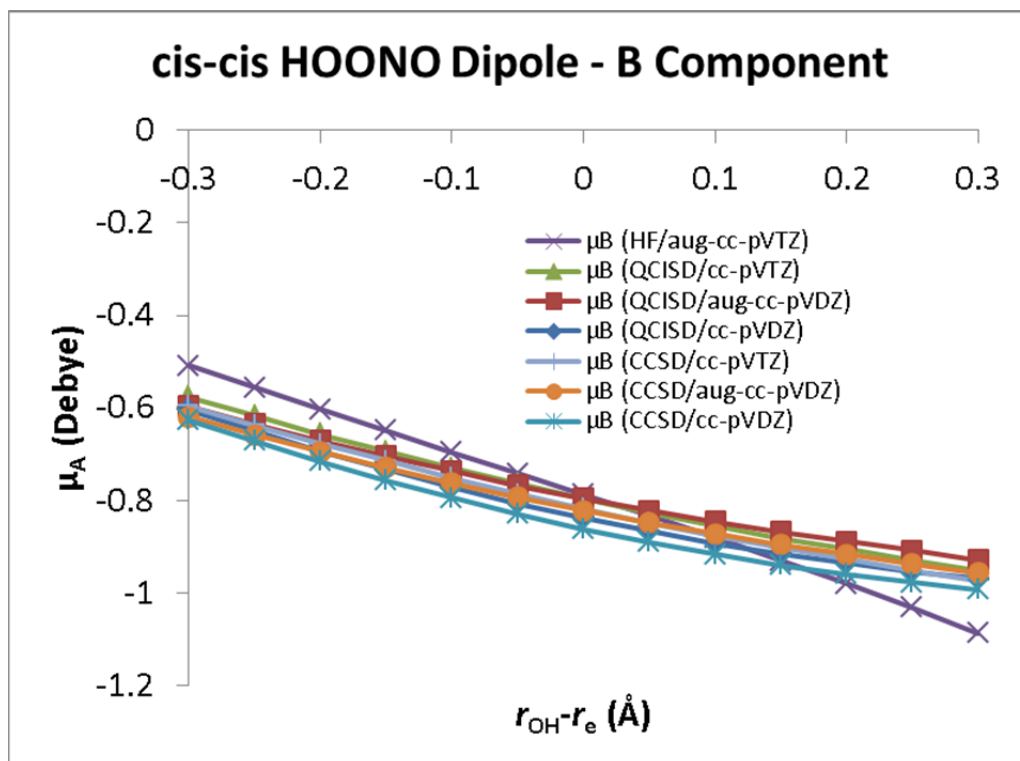


Figure 3.7. μ_b (Debye) for cis-cis HOONO, for $r_{OH} = r_e - 0.3 \text{ \AA}$ to $r_e + 0.3 \text{ \AA}$, at seven combinations of level of theory and basis. The HF/aug-cc-pVTZ data are taken from McCoy et al.⁴² The dipole value and dipole derivative are sensitive to both the level of theory and basis set. The HF-aug-cc-pVTZ dipole derivative is larger than any of the other methods. The QCISD and CCSD methods produced dipole components in relatively good agreement with each other, although the dipole derivatives for the aug-cc-pVDZ calculations were 10% lower than the cc-pVDZ and cc-pVTZ calculations.

We are able to select an appropriate method for calculating the dipole moment surface by considering the dipole moment data in Tables 3.2 and 3.3, and Figures 3.6 and 3.7. We first note that the HF/aug-cc-pVTZ dipole components do not qualitatively or quantitatively agree with the higher levels of theory (CCSD, QCISD). While the QCISD and CCSD plots of μ_A and μ_B vs r_{OH} are roughly the same shape across all basis sets, the HF plots show a much steeper slope, and therefore a larger dipole derivative. Additionally, the absolute magnitudes of the HF dipoles differ from the QCISD and CCSD dipoles: across the entire plot for the A component, and for small and large r_{OH} for the B component. **For these reasons, we therefore conclude that the HF/aug-cc-pVTZ**

dipole surface used by McCoy et al. is inadequate for modeling the spectroscopy of HOONO.

Next, consider the effect of changing the basis set. For both the A and B dipole components, increasing the basis beyond cc-pVDZ changes the dipole moment values and dipole derivative. This indicates that we have to use a larger basis set than cc-pVDZ. The dipole magnitude and dipole derivative for the A component is basically unaffected by choosing aug-cc-pVDZ or cc-pVTZ. The same does not hold true for the B component. Near $r_{\text{OH}} = r_e$, the dipole magnitudes are roughly equal. However, the dipole derivatives are different: cc-pVTZ gives a dipole derivative equal to cc-pVDZ, while aug-cc-pVDZ is lower by 10%. It is likely that the extra flexibility of the augmented basis set (polarization and diffuse functions) is necessary to model HOONO, especially given the change in the B component of the dipole as these functions are added. **We therefore choose to use the aug-cc-pVDZ basis set to model our dipole moment surface.**

The final consideration is whether to use QCISD or CCSD. CCSD is generally considered to be a more accurate level of theory than QCISD;⁹⁵ however, CCSD is also more computationally expensive. Given our computational resources, if the CCSD surface would take too long to calculate, we would be left with no choice but to use QCISD. Gaussian Inc. does not allow us to make any timing data public as part of our license agreement. What we can state is that the CCSD calculations were more expensive than the QCISD calculations by about a factor of 2, and that this factor did not put the CCSD calculations out of our reach. **Therefore, we chose to run the dipole moment surface at CCSD/aug-cc-pVDZ.**

Wavefunctions

Figure 3.8 shows the first 8 wavefunctions obtained from the torsional potential energy surface. The states are denoted as $(n_{\text{HOON}}, n_{\text{OONO}})$, representing the number of quanta of energy in each torsional mode. Each plot shows the potential energy surface contours from Figure 3.3 underneath the wavefunctions. There are two key features of these wavefunctions to note. First, the wavefunctions confirm the observations we made from the potential energy surface regarding the torsional mode coupling. The wavefunctions are off-axis near the bottom of the potential well, giving us another indication of the coupling between the two torsional modes. This is illustrated best in the ground state, $(1, 0)$, and $(0, 1)$ wavefunctions. As we move away from the potential minimum, the wavefunctions move back to being on-axis, representing the uncoupling of the normal modes due to breaking of the internal hydrogen bond. This is best illustrated in the $(4, 0)$ and $(5, 0)$ wavefunctions. Second, we notice a buildup of wavefunction intensity in the cis-perp region for many of the excited states: $(2, 0)$, $(3, 0)$, $(4, 0)$, $(5, 0)$, and $(1, 1)$. The large amount of intensity indicates that these states will have cis-perp character, despite the fact that there is no cis-perp minimum on our surface, supporting the experimental studies that indicate the spectroscopic importance of the cis-perp conformer.

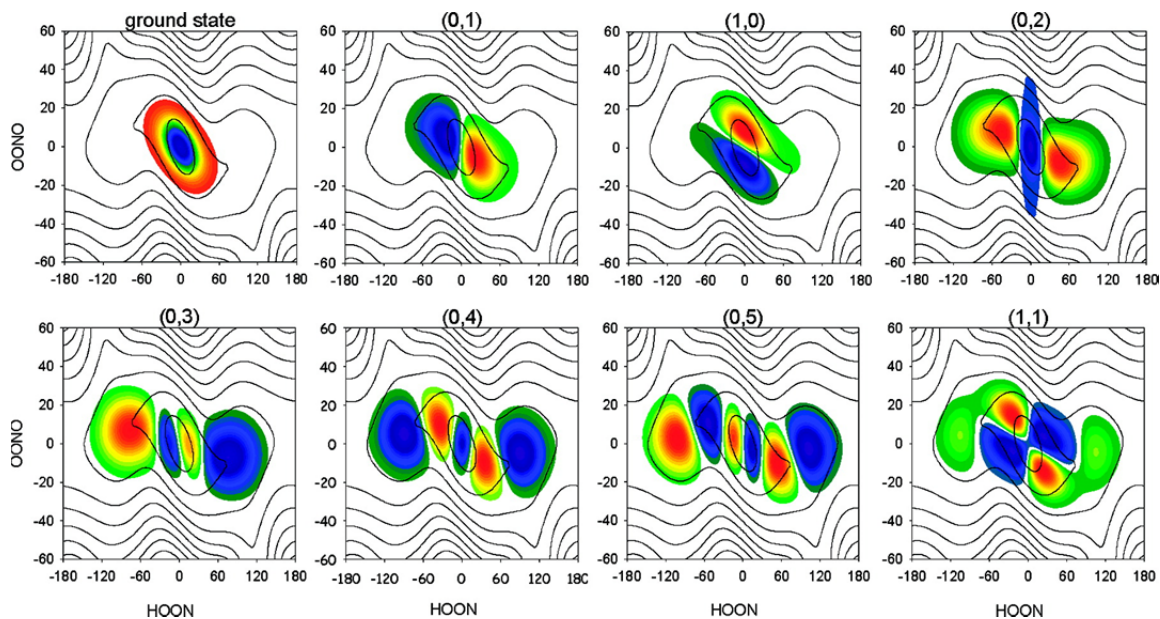


Figure 3.8. Wavefunctions for the 8 lowest energy torsional states of HOONO overlaid on the potential energy surface from Figure 3.3. The labels for each wavefunction are of the form $(n_{\text{HOON}}, n_{\text{OONO}})$, representing the quanta of energy in each torsional mode. Near the potential energy minimum, the wavefunctions are off-axis, indicating coupling between the two torsional modes. Further from the potential energy minimum, the wavefunctions return to being on-axis, indicating decoupling of the two torsional modes. The (2, 0), (3, 0), (4, 0), (5, 0), and (1, 1) states show a buildup of wavefunction intensity in the cis-perp region ($\tau_{\text{HOON}} = 90^\circ$, $\tau_{\text{OONO}} = 0^\circ$). Reprinted with permission from McCoy et al.⁴³ Copyright 2010 American Chemical Society.

Discussion

Simulated OH Stretch Spectra (Fundamental, Overtone)

Simulations of the OH stretch spectra of HOONO based on our 3-dimensional potential energy surface were carried out by Professor Anne McCoy.⁴³ The results are shown here to illustrate the effects of using our new potential energy surface and dipole moment surface. Figure 3.9 shows two simulations for the fundamental spectrum (left) and first overtone spectrum (right). The black lines are the spectra obtained using the 3-dimensional PES and dipole moment surface presented in this chapter. The blue lines are

the spectra obtained from a reduced (2-dimensional) potential energy surface, varying τ_{HOON} , and letting τ_{OONO} relax along the minimum energy path.

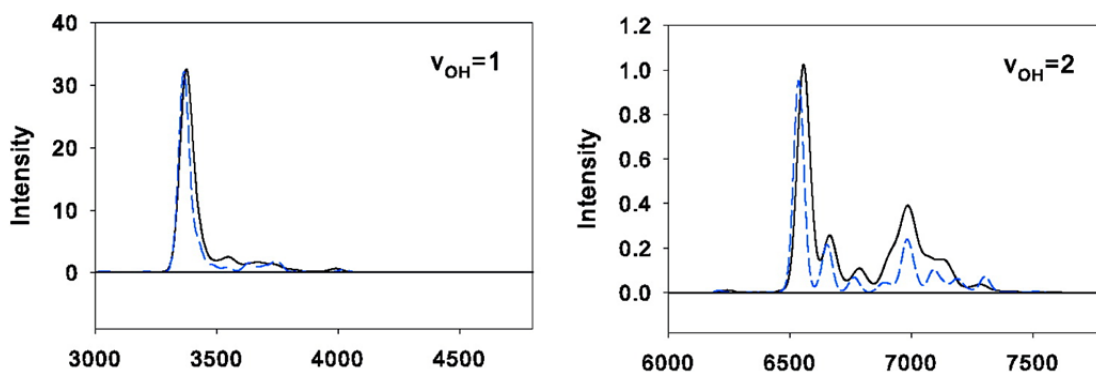


Figure 3.9. Calculated OH stretch spectra for HOONO based on our CCSD(T)/cc-pVTZ potential energy surface (Figure 3.3) and our CCSD/aug-cc-pVDZ dipole moment surface. The fundamental is shown in the left panel, while the first overtone is shown in the right panel. Spectra are convoluted with a 60 cm^{-1} Gaussian. Black line: fit to full 3-dimensional surfaces. Blue line: reduced dimensionality (2-dimensional, minimum energy path as a function of τ_{HOON}). Sequence band intensity is observed in all spectra, with significant intensity observed in the overtone spectrum. Reprinted with permission from McCoy et al.⁴³ Copyright 2010 American Chemical Society.

We note the following key features of the spectra in Figure 3.9. First, significant OH stretch intensity is found in sequence bands, roughly the same fraction whether the 2-dimensional or 3-dimensional PES is used. However, the shape of the sequence band spectrum is different between the two surfaces. This is most apparent in the overtone spectrum (right panel of Figure 3.9). Second, a greater fraction of intensity is found in the sequence bands for the overtone spectrum compared to the fundamental spectrum. This is a direct result of accessing the cis-perp shelf in the overtone spectrum. Third, the reduced dimensionality treatment (blue line) underestimates the fraction of intensity in the sequence bands. This illustrates the point that explicitly accounting for τ_{OONO} is necessary to develop an accurate picture of HOONO spectroscopy.

Torsional Spectrum

On the basis of our 2-dimensional potential energy surface (τ_{HOON} , τ_{OONO}) shown in Figure 3.3, we can simulate the pure torsional spectrum of HOONO and DOONO. In Figure 3.10, we compare our simulated torsional stick spectra (bottom) to the matrix IR spectra of HOONO (left) and DOONO (right) of Zhang et al.¹⁶ Zhang's band assignments are marked on their matrix spectra. Since our potential energy surface only is a function of τ_{HOON} and τ_{OONO} , we only obtain ν_9 (ν_{HOON}) and ν_8 (ν_{OONO}) transitions; the simulated spectra do not contain any ν_4 , ν_5 , ν_6 , or ν_7 lines. Previous work has shown that the $\nu_8 + \nu_9$ intensity is equal to the ν_4 intensity.¹⁶ We have scaled the matrix and calculated spectra to reflect this.

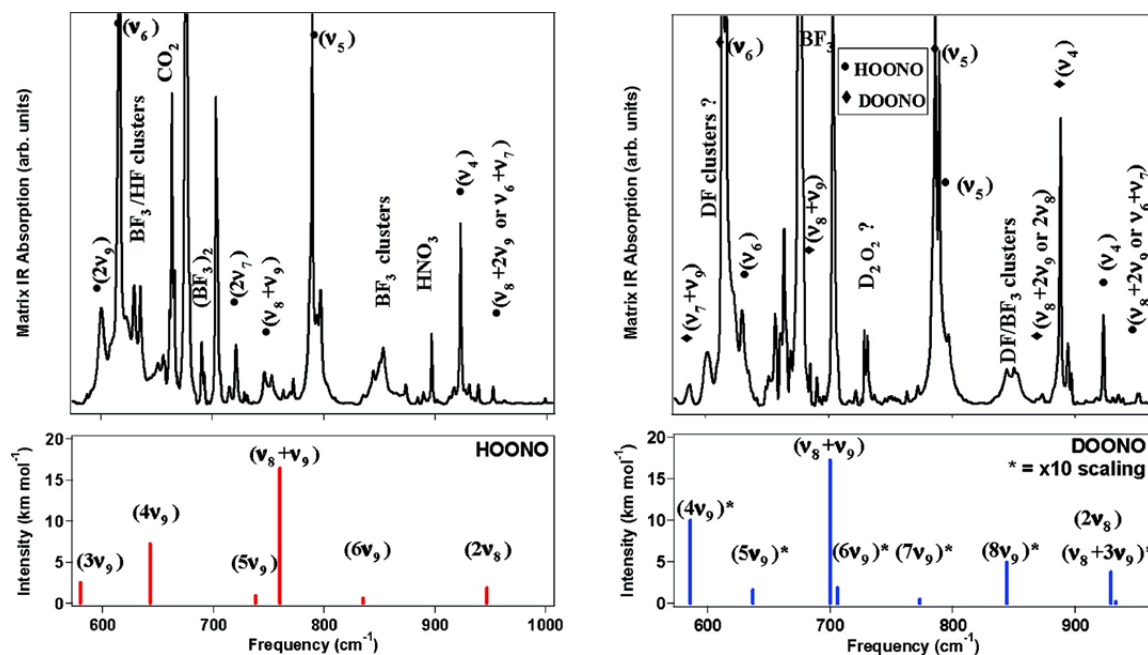


Figure 3.10. Simulated torsional spectrum (bottom) and experimental matrix spectra (top)¹⁶ for HOONO (left) and DOONO (right). The simulated spectra are based off of our CCSD(T)/cc-pVTZ potential energy surface (Figure 3.3), and only contain transitions involving ν_9 (ν_{HOONO}) and ν_8 (ν_{DOONO}). Zhang's assignments are marked on the matrix spectra. The matrix spectra have been scaled so that the calculated $\nu_8+\nu_9$ frequency is equal to the observed ν_4 frequency.¹⁶ Transitions marked with an asterisk have been scaled up by a factor of 10 to improve visibility. Reprinted with permission from McCoy et al.⁴³ Copyright 2010 American Chemical Society.

While many of the simulated bands fall within dense clusters of other peaks, we can suggest two reassignments based on our simulated spectra. First, Zhang et al. assign their HOONO band at 601 cm^{-1} to $2\nu_9$ on the basis of VPT2 calculations.¹⁶ Our simulated spectra suggest that this band should be assigned to $3\nu_9$ (calculated from our PES at 580 cm^{-1}). Second, we suggest that the observed DOONO band at 950 cm^{-1} arises from a combination of $2\nu_8$ and $\nu_8+3\nu_9$, two states that heavily mix.⁴³ It is unlikely that these bands arise from $\nu_8+2\nu_9$ as assigned by Zhang *et al.* because of the large difference between the calculated frequency (863 cm^{-1}) and observed band (950 cm^{-1}). It is more likely that Zhang's assignment of their peak at 870 cm^{-1} to $\nu_8+2\nu_9$ is correct.

Correction factor to $\alpha(p, 298K)$

One of the goals of our study was to determine the extent to which sequence band formation would affect spectroscopic measurements of the OH + NO₂ branching ratio (Reactions 3.1 and 3.2). As stated in the Introduction, any HOONO intensity that is in its sequence bands will not be accounted for, and [HOONO] will be underestimated. To correct for this, we modify Equation 3.4 to reflect our interpretation of the CRDS experiment:

$$\alpha(298K, p) = \frac{\int_{3250 \text{ cm}^{-1}}^{3400 \text{ cm}^{-1}} A_{HOONO} d\bar{\nu}}{\int_{3480 \text{ cm}^{-1}}^{3620 \text{ cm}^{-1}} A_{HONO_2} d\bar{\nu}} \times \frac{\sigma_{HONO_2}}{\sigma_{HOONO}} \times K_{CRDS} \times K_{seq, 3400, 298K}, \quad (3.13)$$

where K_{CRDS} corrects for nonlinearities in the measured absorbances,³⁰ and $K_{seq, 3400, 298K}$ is the correction factor for HOONO sequence band intensity at frequencies above 3400 cm⁻¹ at 298 K. The integral limits are the same limits used by Mollner et al. in their experiment.³⁰

On the basis of the OH stretch fundamental spectrum in Figure 3.9, we determine 17% of the HOONO intensity to be in sequence bands at frequencies greater than 3400 cm⁻¹. This value is slightly greater than McCoy's value of 15% based on their 2-dimensional potential energy surface:⁴² another indication that inclusion of the OONO torsional mode in our theoretical treatment of HOONO impacts the derived energy levels, spectroscopy, and interpretations of experiments. We therefore set $K_{seq, 3400, 298K} = 1.17$, and use this value for Mollner's calculation of $\alpha(298 \text{ K}, p)$.³⁰

Conclusions

In this chapter, we have reported a 3-dimensional potential energy surface at the CCSD(T)/cc-pVTZ level of theory and basis and a 3-dimensional dipole moment surface at the CCSD/aug-cc-pVDZ level of theory and basis for peroxyxynitrous acid (HOONO). These surfaces are functions of the two torsional modes (ν_{HOON} , ν_{OONO}) and the OH stretch mode (ν_{OH}). Significant coupling between the HOON and OONO torsions is observed on the torsional potential energy surface near the cis-cis minimum. The derived wavefunctions also show coupling near the cis-cis minimum, and considerable intensity buildup near the cis-perp shelf for when energy is placed into the HOON torsion. The simulated vibrational and torsional spectra obtained from our surfaces were used to assess sequence band formation, revise assignments to previous matrix spectra of HOONO, and interpret cavity ringdown spectroscopy measurements of the branching ratio of OH + NO₂.

Acknowledgements

We thank Professor Anne McCoy for fitting of the potential energy surface, calculation of wavefunctions, simulated spectra, and provision of computer time for this project, Sara Ray for patience and assistance with running calculations on the Ohio State server, Andrew Mollner and Markus Keller for initial geometry and energy calculations, Jonathan Chen for installation of Q-Chem on the Okumura group server, and NASA/JPL for provision of computer time for this project. The experiments performed in this chapter were funded under NASA Upper Atmosphere Research Program Grants NAG5-11657, NNG06GD88G, and NNX09AE21G2, California Air Resources Board Contract 03-333

and 07-730, National Science Foundation CHE-0515627, and a Department of Defense National Defense Science and Engineering Graduate Fellowship (NDSEG).